Pulsewidth Modulation Strategy in Double-Delta Sourced Winding

Yongsoon Park [ORCID], *Member, IEEE* and Seung-Ki Sul [ORCID], *Fellow, IEEE*

Abstract—**Power conversion systems based on double-delta sourced winding (DDSW) had an optimization issue in terms of pulsewidth modulation (PWM). This issue was about inefficient employments of voltage levels during PWM and had to be considered for minimizing voltage stresses and current ripples on DDSW. In this paper, a novel method has been proposed to improve the performance of PWM in DDSW-based systems. The proposed method can be simply implemented as a carrier-based PWM and its principles are neatly summarized with equations. Finally, the effectiveness of the proposed method is demonstrated with experimental results, which were obtained by using a transformer and an induction machine.**

Index Terms—**Double-delta sourced winding, multilevel converter, pulsewidth modulation.**

NOMENCLATURE

Abbreviations

CNV	Converter.
SOV	Single-one vector.
SZV	Single-zero vector.
SS	Subsector in the combined voltage plane.

Variables

S_a, S_b, S_c	Switching functions of a, b, c.
S_r, S_s, S_t	Switching functions of r, s, t.
T_{mod}	Modifying time (pivoting time).
T_{comp}	Compensating time ($= T_{\mathrm{mod}}$).
$\mathrm{T}_{\mathrm{samp}}$	Sampling time for current regulation.
$\overrightarrow{\mathrm{V}}$	Voltage vector.
V_{dc}	DC-link voltage of converter.
V_{max}	Maximum reference.
V_{med}	Medium reference.
V_{min}	Minimum reference.

Subscripts

$\alpha p, \beta p, \gamma p$	Phases of primary winding.
$\alpha 1, \beta 1, \gamma 1$	Phases of secondary winding #1.
$\alpha 2, \beta 2, \gamma 2$	Phases of secondary winding #2.
a, b, c	Phases of converter X.
r, s, t	Phases of converter Y.
co	Combined voltage at the primary side by converters.
X	Converter X (a, b, c).
Y	Converter Y (r, s, t).
zs	Zero sequence.

Superscripts

$*$	Reference.
p	Pivoting mode.
e	Enclosing mode.

I. INTRODUCTION

THE POWER conversion based on double-delta sourced winding (DDSW) is helpful to mitigate undesirable harmonics at switching frequency [1]–[3]. In DDSW, the outputs of two three-phase converters are combined through six windings, and the interleaved structure can improve harmonic properties over the entire system. This scheme is attractive in high-power systems where multiple windings and converters are naturally required for power sharing [4]–[6]. The DDSW can be easily implemented in the power conversions using a transformer or an electrical machine. In specific, the regulation of active and reactive powers to a grid had been shown through a DDSW-based transformer [2], and the vector control had been demonstrated with a DDSW-based induction machine [3].

The conventional method for pulsewidth modulation (PWM) of DDSW is based on the simple interleaving method using phase shift of carrier waves [1], [7]. Namely, the carrier waves used for PWM in DDSW are out of phase by 180° to each other as shown in Fig. 1, where the same three-phase reference is assumed for the converters denoted by CNV_X and CNV_Y. By virtue of this interleaving in conjunction with DDSW, the number of voltage levels applied to the windings could be increased from three to nine as presented in Fig. 2 [1]. It was also shown that the winding voltages at the same phase, $v_{\alpha 1}$ and $v_{\alpha 2}$ in Fig. 2, had phase-shifted ripples at switching frequency even if their fundamentals were in phase. These sorts of ripples are inevitable unless the voltage level of converter is infinite.

The ripples caused by PWM should be minimized as much as possible in order to reduce filtering and losses. However, the
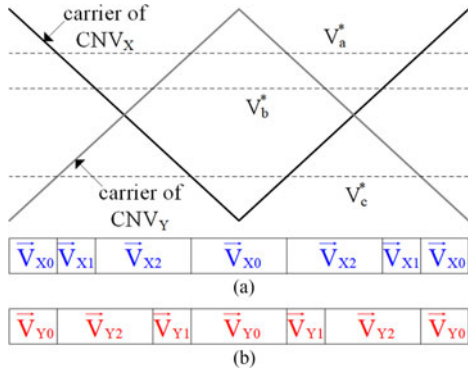
Fig. 1. Conventional interleaving method using carrier-based PWM. (a) Space-vector application for CNV_X. (b) Space-vector application for CNV_Y.
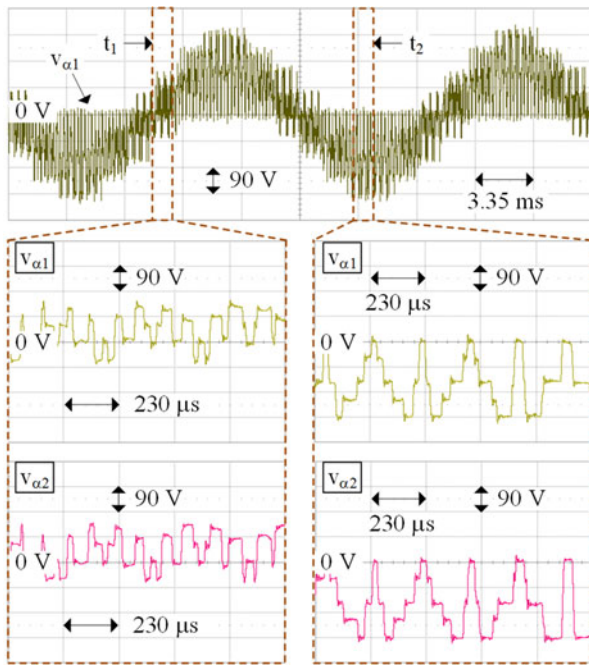

Fig. 2. Winding voltages by conventional PWM [1].

Fig. 3. Structure of DDSW.

Fig. 4. Per-phase circuit on A-phase.

conventional PWM method for DDSW cannot be regarded as the optimal solution in this respect. As evidence, the magnitudes of PWM ripples around t_1 and t_2 are very different in Fig. 2. That is, too many levels may be employed at some instants for the voltage synthesis in the conventional PWM method. Therefore, the purpose of this paper was to optimize the employment of voltage levels for PWM in DDSW-based systems.

In this paper, a new concept of PWM for DDSW is proposed and described with respect to the implementation. After it is reviewed why the conventional method is not optimal, the principle to resolve this problem is detailed in a vector space, and its implementation is suggested in a way to use carrier waves for PWM. Finally, the effectiveness of the proposed method is demonstrated with experimental results.

II. COMBINED VOLTAGE OUTPUTS IN DDSW

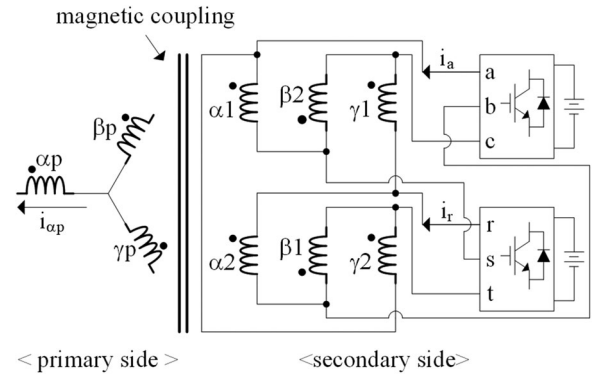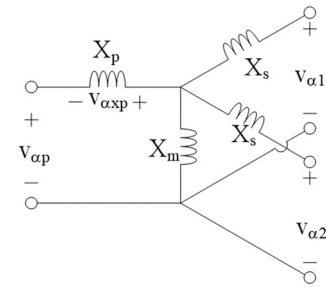The structure of DDSW-based systems can be explained with Fig. 3. The power conversion circuit is divided into primary and secondary sides by magnetic coupling. In particular, the harmonic property at the primary side is important in evaluating the quality of power conversions. For instance, the primary side is connected to an ac grid in transformer applications. In order to this grid connection, associated harmonic regulations should be satisfied at the primary side [8]. Therefore, the combined influence of the converters at the primary side should be considered for PWM's optimization. The following explanations are mainly developed by assuming a DDSW-based transformer connected to a grid for easy understanding.

The combined output at the primary side can be regarded as the summation of voltage outputs from each converter of the secondary side. For better understanding, the per-phase analysis shown in Fig. 4 can be used if a DDSW-based transformer has balanced impedances [9]. At first, the magnetizing reactance (X_m) is normally large enough to ignore. In addition, if each secondary leakage reactance (X_s) is double the primary leakage reactance (X_p) in per unit, then the voltage drop on the primary leakage reactance $(v_{\alpha xp})$ can be derived as (1).

$$v_{\alpha xp} = \frac{1}{4}(v_{\alpha 1} + v_{\alpha 2} - 2v_{\alpha p}) \tag{1}$$

where $v_{\alpha 1}$ and $v_{\alpha 2}$ are applied by the converters at the secondary side, and $v_{\alpha p}$ is applied by a grid voltage at the primary side.

The current flowing into the grid is affected by the converter voltages and the grid voltage, as presented in (1). The grid voltage is normally given, whereas the converter voltages can be adjusted. By the superposition principle, only the converter voltages can be separately considered for optimizing PWM.

The combined voltage outputs at the primary side by the converters can be expressed with (2) if the analysis per phase is
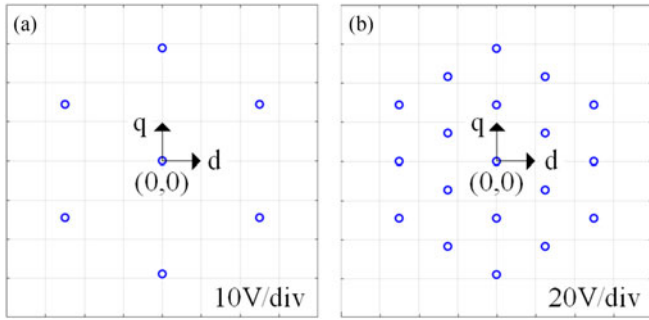
Fig. 5. Space vectors in combined d–q plane: (a) voltage vectors from each converter; and (b) combined voltage vectors.

considered altogether for three phases.

$$\begin{bmatrix} v_{\alpha xp\_co} \\ v_{\beta xp\_co} \\ v_{\gamma xp\_co} \end{bmatrix} = \frac{1}{4} \left(\begin{bmatrix} v_{\alpha 1} \\ v_{\beta 1} \\ v_{\gamma 1} \end{bmatrix} + \begin{bmatrix} v_{\alpha 2} \\ v_{\beta 2} \\ v_{\gamma 2} \end{bmatrix} \right) \qquad (2)$$

Space vectors can be considered in a d–q voltage plane for the optimal PWM of the combined outputs. In order to identify which space vectors are used, the winding voltages in (2) should be specified with respect to the switching functions [1], [10]. After the winding voltages are expressed with switching functions by the literature [1], the d–q voltage of the combined output is derived as (3a) from (2) by Clarke's transformation of (3b)

$$\begin{bmatrix} v_{d\_co} \\ v_{q\_co} \end{bmatrix} = T_{cl} \cdot \begin{bmatrix} v_{\alpha xp\_co} \\ v_{\beta xp\_co} \\ v_{\gamma xp\_co} \end{bmatrix} = A_1 \cdot \begin{bmatrix} S_a \\ S_b \\ S_c \end{bmatrix} + B_1 \cdot \begin{bmatrix} S_r \\ S_s \\ S_t \end{bmatrix}$$

$$= \begin{bmatrix} v_{Xd} \\ v_{Xq} \end{bmatrix} + \begin{bmatrix} v_{Yd} \\ v_{Yq} \end{bmatrix} \qquad (3a)$$

where

$$T_{cl} = \frac{2}{3} \cdot \begin{bmatrix} 1 & -1/2 & -1/2 \\ 0 & \sqrt{3}/2 & -\sqrt{3}/2 \end{bmatrix} \qquad (3b)$$

$$A_1 = B_1 = \frac{V_{dc}}{4} \cdot \begin{bmatrix} 1 & -1 & 0 \\ 1/\sqrt{3} & 1/\sqrt{3} & -2/\sqrt{3} \end{bmatrix}. \qquad (3c)$$

In the above equations, the dc-link voltages of the converters are equally assumed as V_{dc}. Because S_a, S_b and S_c are related to CNV_X, and S_r, S_s, and S_t are related to CNV_Y, d–q components by each converter can be denoted by v_{Xd}, v_{Xq}, v_{Yd}, and v_{Yq}.

The coordinates of the space vectors are identified by inserting 1 or 0 into each switching function in (3), and indicated in the combined voltage plane as shown in Fig. 5 when V_{dc} is 100 V. Because the line-to-line voltages of the converters are applied to the windings of DDSW, the space vectors present the variations of 30° and $\sqrt{3}$ in phase and magnitude, respectively. When considering Fig. 5(a) and (b), it is inferred that the combination of two converters by DDSW results in the distribution of space vectors similar to that of three-level converters [11].

As a similar case, the open-end winding is comparable to DDSW in which two converters are combined for one power
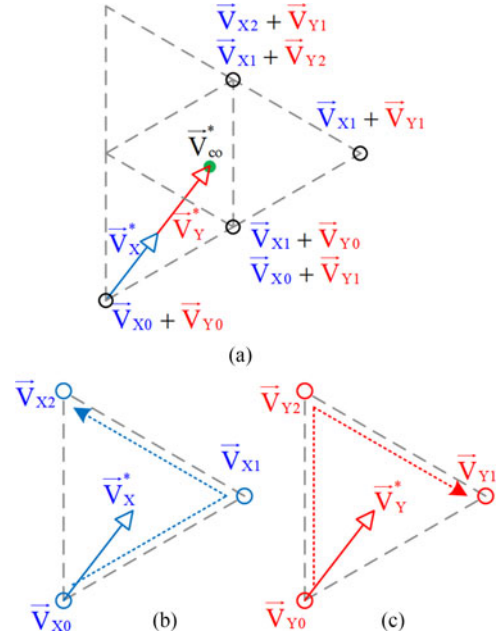

Fig. 6. Employment of space vectors in the conventional PWM: (a) combined vectors; (b) CNVx vectors; and (c) CNVy vectors.

conversion [12], [13]. In the open-end winding, after the combined voltage reference is determined for the current regulation at the fundamental frequency, each converter's reference can be aptly assigned for PWM, such that the combined reference is not changed. There exist some options to optimize PWM by adjusting each converter's output because only their combined output is important for the current regulation. However, in the case of DDSW, each converter's output is determined at first for the current regulation, and their combined output is automatically decided. That is, if each converter's reference in DDSW is arbitrarily adjusted for an optimal PWM, the current regulation may be disturbed. The purpose of this paper is to propose an optimal PWM method without disturbing the current regulation.

The reason why the conventional PWM for DDSW is not optimal can be clearly understood in the combined voltage plane. For simplicity, each converter's reference is assumed to be identical, which is quite effective in grid applications because the grid voltage accounts for almost portion of voltage reference. The employment of space vectors by the conventional PWM is shown in Fig. 6 as an example. In the figure, even if each converter has the same reference vector ($\vec{V}_X^* = \vec{V}_Y^*$), the applying sequences of space vectors are opposite due to the interleaving, which can be explained from the space-vector applications in Fig. 1. In Fig. 6, while PWM is carried out with the nearest three vectors in the respective converters, it does not in the view point of the combined voltage reference $\vec{V}_{co}^*$. The space vectors used to synthesize $\vec{V}_{co}^*$ in the conventional PWM are indicated by circles in Fig. 6(a). Those vectors are not the closest group to $\vec{V}_{co}^*$, and they are many in number. Therefore, the combined voltage reference needs to be synthesized with the nearest three vectors.

The key element for the optimization of PWM is dividing the roles of each converter in DDSW. These roles are distinguished by what types of space vectors are applied by the converter. In
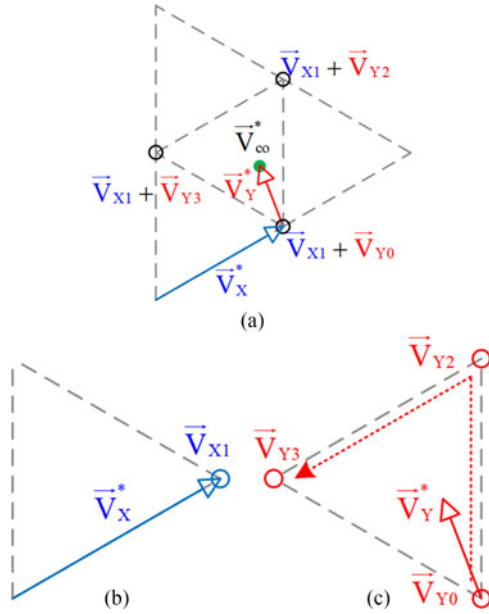
Fig. 7. Employment of space vectors in the proposed PWM: (a) combined vectors; (b) CNVx vectors; and (c) CNVy vectors.

Fig. 8. Distribution of SOVs and SZVs in DDSW.

Fig. 9. Carrier-based PWM during T_{samp}.

Fig. 7, the example is shown with respect to the same reference $\vec{V}_{\mathrm{co}}^*$. In order to use the nearest three vectors to $\vec{V}_{\mathrm{co}}^*$, one converter (CNV_X) applies a pivot vector whereas the other (CNV_Y) applies enclosing vectors. By virtue of this role distribution, it is expected to reduce the excessive usage of voltage levels during PWM. Even though the voltage references are modified for the role distribution, it is very important to conserve the original volt-second outputs for the current regulation.

III. PROPOSED PWM

A. Fundamental Concepts to Generalize PWM

General concepts have to be defined for simple explanation of the proposed method. In particular, those can be helpful to minimize pointless repetition of similar explanation in PWMs. In addition, generalized discussion can prevent deducing a restricted solution for certain conditions. In this paper, the implementation of the proposed method can be easily derived, thanks to these sorts of general concepts.

The space vectors made by each converter can be represented by their three-phase switching functions. At one phase leg, if the upper switch is ON, its switching function is defined as unity [10]. Otherwise, the switching function becomes zero. If three-phase legs are considered at once, the three-phase switching function is expressed with three binary digits. Because space vectors by a two-level converter form a hexagon [14], the three-phase switching functions are indicated on the voltage hexagon. Due to the phase shift described in Fig. 5, the space vectors applied by each converter in DDSW can be depicted as shown in Fig. 8.

The space vectors in Fig. 8 can be classified by the property of three-phase switching function. Namely, if only one digit of the three-phase switching function presents unity, it is defined as a single-one vector (SOV). In addition, if only one digit presents
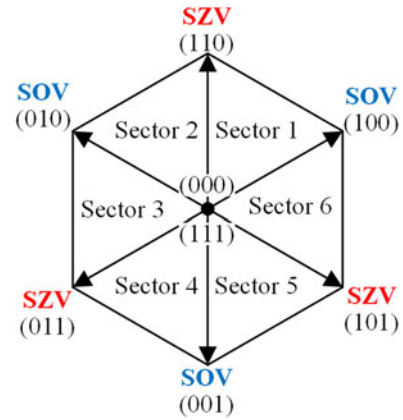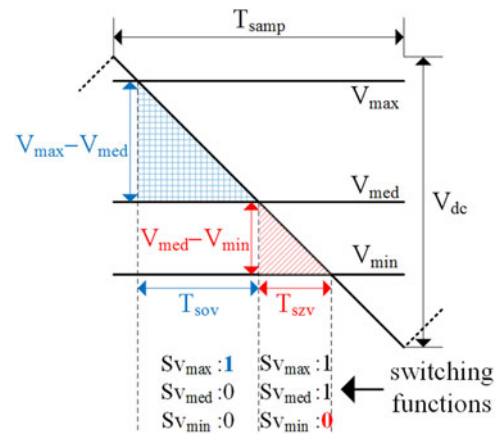
zero, it is defined as a single-zero vector (SZV). If a space vector is neither SOV nor SZV, it must be the zero vector whose magnitude is null for PWM.

The space vector modulation (SVM) can be generalized with the concept of SOV and SZV. This is because every effective vector, whose magnitude is not null, must be either SOV or SZV, and every sector in Fig. 8 is separated by one set of SOV and SZV. That is, if the concept of SOV and SZV is employed, SVM can be described regardless of the sector where a reference vector lies. In combination with the conventional formula [15], SVM with respect to a reference vector $\vec{V}^*$ can be generalized with the following equation:

$$\vec{V}^* = \frac{1}{T_{\mathrm{samp}}}(\vec{V}_{\mathrm{sov}} \cdot T_{\mathrm{sov}} + \vec{V}_{\mathrm{szv}} \cdot T_{\mathrm{szv}}) \tag{4}$$

where T_{sov} and T_{szv} are the application times of SOV and SZV during T_{samp}, which means a sampling time.

The voltage synthesis in (4) can be implemented with a carrier wave as shown in Fig. 9 [16]. With the concept of SOV and SZV, it is not important to clarify the phases of voltage references but their relative magnitudes. That is, as shown in Fig. 9, when only V_{max}, which is the maximum reference, is over the carrier wave, SOV is applied by the converter. On the other hand, when only V_{min}, which is the minimum, is below the carrier wave, SZV is applied. Therefore, the application times of SOV and SZV are

determined by the magnitude differences of voltage references. Therefore, as presented in Fig. 9, T_{sov} is proportional to $V_{\max} - V_{\text{med}}$, whereas T_{szv} to $V_{\text{med}} - V_{\min}$. This fact rearranges (4) into the following equation:

$$\vec{V}^* = \frac{1}{T_{\text{samp1}}} \cdot \frac{T_{\text{samp2}}}{V_{\text{dc}}} \cdot \left\{ \vec{V}_{\text{sov}} \cdot (V_{\max} - V_{\text{med}}) \right.$$
$$\left. + \vec{V}_{\text{szv}} \cdot (V_{\text{med}} - V_{\min}) \right\} \tag{5}$$

where T_{samp1} and T_{samp2} are actually the same as T_{samp} but just used for distinction. Hereafter, T_{samp} indicates the sampling time for the current regulation, which is synchronized with the carrier wave.

Equation (5) means that a reference vector can be synthesized during T_{samp1} with a three-phase reference and a triangular wave whose slope is $V_{\text{dc}}/T_{\text{samp2}}$. Based on (5), the implementation of the proposed PWM can be easily described.

B. Carrier-Based PWM by the Proposed Method

The voltage references to achieve the current regulation have to be modified to optimize PWM of DDSW, as explained in Fig. 7. However, in order not to disturb the current regulation, the original volt-second intended by the initial references must be preserved within T_{samp}. In other words, if a voltage reference is modified during some period of T_{samp}, its volt-second change has to be compensated during the rest of T_{samp}. The modifying time T_{mod} can be set equal to the compensating time T_{comp}. Because the sum of T_{mod} and T_{comp} is T_{samp}, it can be summarized as the following equation:

$$T_{\text{mod}} = T_{\text{comp}} = T_{\text{samp}}/2. \tag{6}$$

Equation (7) is derived by inserting (6) into (5) because T_{samp1} and T_{samp2} are equal to T_{samp} as mentioned earlier. Although the following explanations are discussed with respect to CNV_X, the same procedures are applied to CNV_Y:

$$\vec{V}_X^* = \frac{1}{2T_{\text{mod}}} \cdot \frac{T_{\text{mod}}}{V_{\text{dc}}}$$
$$\times \left\{ \vec{V}_{\text{sov}} (2V_{\max} - 2V_{\text{med}}) + \vec{V}_{\text{szv}} (2V_{\text{med}} - 2V_{\min}) \right\}. \tag{7}$$

From the comparison with (5), it is inferred from (7) that a reference vector can be synthesized during $2T_{\text{mod}}$ with a triangular-wave whose slope is $V_{\text{dc}}/T_{\text{mod}}$. This is a direct hint to implement the proposed method as a carrier-based PWM.

The three-phase reference in (7) needs to be considered in their voltage plane. Naturally, the space vector of $2V_{\max}, 2V_{\text{med}}$, and $2V_{\min}$ is two times that of $V_{\max}, V_{\text{med}}$, and $V_{\min}$ in the same direction. Therefore, it is plausible to divide this enlarged vector into two small vectors for optimizing PWM. Namely, one of them is used as a pivot vector for one T_{mod}, whereas the other is used to apply enclosing vectors for the other T_{mod}. Because each small vector would be synthesized by one set of SOV and SZV as explained with (4) and (5), (7) finally has to
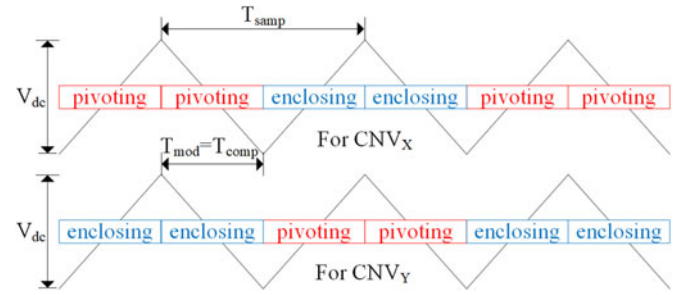

Fig. 10. Carrier-based implementation of proposed method.

be rearranged as

$$\vec{V}_X^* = \frac{1}{2T_{\text{mod}}} \frac{T_{\text{mod}}}{V_{\text{dc}}} \left\{ \vec{V}_{\text{sov}}^p (V_{\max}^p - V_{\text{med}}^p) + \vec{V}_{\text{szv}}^p (V_{\text{med}}^p - V_{\min}^p) \right.$$
$$\left. + \vec{V}_{\text{sov}}^e (V_{\max}^e - V_{\text{med}}^e) + \vec{V}_{\text{szv}}^e (V_{\text{med}}^e - V_{\min}^e) \right\} \tag{8}$$

where superscript "p" indicates the pivoting mode, whereas superscript "e" designates the enclosing mode.

The core of the proposed method is how to calculate two sets of three-phase references for each mode in (8) from the original references ($V_{\max}, V_{\text{med}}$, and $V_{\min}$) in (7). In fact, if $V_{\max}^p, V_{\text{med}}^p$, and $V_{\min}^p$ are determined; $V_{\max}^e, V_{\text{med}}^e$, and $V_{\min}^e$ are naturally computed because the total volt-second outputs must be fixed by (7) during $2T_{\text{mod}} (= T_{\text{samp}})$. As a consequence, if a modification is made to apply a pivot vector, it is compensated by applying enclosing vectors.

The carrier wave used for the proposed method changes by V_{dc} per T_{mod} because it has the slope of $V_{\text{dc}}/T_{\text{mod}}$, as discussed in (7). Since a pole voltage reference is compared with the carrier wave whose peak-to-peak is equal to the dc-link voltage in a two-level converter, the proposed PWM can be implemented as shown in Fig. 10 with the carrier wave whose peak-to-peak is V_{dc} and period is $T_{\text{samp}} (= 2T_{\text{mod}})$. In the figure, $V_{\max}^p, V_{\text{med}}^p$, and $V_{\min}^p$ in (8) are used for PWM during the pivoting mode, whereas $V_{\max}^e, V_{\text{med}}^e$, and $V_{\min}^e$ during the enclosing mode.

A combined voltage reference is synthesized with a pivot vector from one converter and enclosing vectors from the other converter. Namely, if one converter is applying a pivot vector, the other converter applies enclosing vectors at the same time. From the perspective of one converter, the transition between the pivoting and enclosing modes has to be occurred during T_{samp} for the current regulation. However, if the transition order is carefully assigned as shown in Fig. 10, the mode transition per $2T_{\text{mod}}$ is available for minimizing switching count. For instance, if an SOV is continuously applied as a pivot vector for $2T_{\text{mod}}$, the three-phase switching function is not changed for this $2T_{\text{mod}}$, which means no switching loss during T_{samp}. However, that sort of continuation cannot be longer than $2T_{\text{mod}}$ because the modification during one T_{mod} should be compensated during the other T_{mod} within one T_{samp}. When considering Fig. 10, PWMs of the converters have been symmetrically designed toward each other, which is generally preferable for better harmonic properties [17].
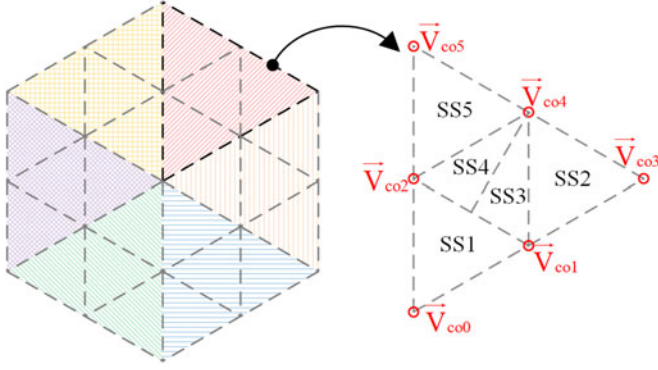
Fig. 11.   Sector divisions in the combined voltage plane.

C. Modification of Voltage References in the Proposed Method

The method to determine three-phase references in (8) varies depending on the relationship among $2V_{\max}, 2V_{\mathrm{med}}$, and $2V_{\min}$ in (7). For easy understanding, as shown in Fig. 11, it is helpful to specify one sector as an example, where a reference vector belongs in the combined voltage plane. One sector is again divided by five subsectors. However, it is noteworthy that the sector determination does not require a heavy calculation for the proposed method. Instead, it is important to identify which phase voltage is $V_{\max}, V_{\mathrm{med}}$, or $V_{\min}$.

Subsector 1 (SS1): The magnitude of pivot vector can be null in SS1 for PWM. This is because any reference vector belongs to SS1 can be synthesized by only one converter's output. By checking (9), it can be detected whether the reference vector is within SS1

$$2V_{\max} - 2V_{\min} < V_{\mathrm{dc}}. \tag{9}$$

In other words, the condition in (9) indicates that the sum of $(2V_{\max} - 2V_{\mathrm{med}})$ and $(2V_{\mathrm{med}} - 2V_{\min})$ is smaller than V_{dc}, and that the total application times of SOV and SZV in (7) is shorter than T_{mod}. Therefore, in the case of SS1, the nearest three vectors can be used for PWM if the voltage synthesis of one converter does not overlap with that of the other converter during $T_{\mathrm{samp}}(=2T_{\mathrm{mod}})$.

The procedure to obtain the three-phase references for each mode begins with the modification shown in the following equation:

$$\vec{V}_X^* = \frac{1}{2T_{\mathrm{mod}}} \frac{T_{\mathrm{mod}}}{V_{\mathrm{dc}}} \left\{ \vec{V}_{\mathrm{sov}} \cdot (2V_{\max} + 0 - 2V_{\mathrm{med}}) \right.$$
$$\left. + \vec{V}_{\mathrm{szv}} \cdot (2V_{\mathrm{med}} + 0 - 2V_{\min}) \right\}. \tag{10}$$

Equation (10) is numerically the same as (7) because the addition of zero is meaningless. However, it can be rearranged into (11) by virtue of this modification

$$\vec{V}_X^* = \frac{1}{2T_{\mathrm{mod}}} \frac{T_{\mathrm{mod}}}{V_{\mathrm{dc}}} \left\{ \vec{V}_{\mathrm{sov}} \cdot 0 + \vec{V}_{\mathrm{szv}} \cdot 0 \right.$$
$$\left. + \vec{V}_{\mathrm{sov}}(2V_{\max} - 2V_{\mathrm{med}}) + \vec{V}_{\mathrm{szv}}(2V_{\mathrm{med}} - 2V_{\min}) \right\}. \tag{11}$$

When the format of (11) is compared with that of (8), the voltage differences for each mode are obtained as (12)

$$\begin{cases} V_{\max}^p - V_{\mathrm{med}}^p = 0 \\ V_{\mathrm{med}}^p - V_{\min}^p = 0 \end{cases} \tag{12a}$$

$$\begin{cases} V_{\max}^e - V_{\mathrm{med}}^e = 2V_{\max} - 2V_{\mathrm{med}} \\ V_{\mathrm{med}}^e - V_{\min}^e = 2V_{\mathrm{med}} - 2V_{\min} \end{cases}. \tag{12b}$$

In summary for PWM in SS1, the original SOV and SZV in (7) are identically used for both the pivoting and enclosing modes as shown in (11), and their application times are proportional to the voltage differences detailed in (12).

The three-phase references compared to the carrier wave are finally determined by adding zero-sequence voltages. For instance, if the phases of $V_{\max}, V_{\mathrm{med}}$, and $V_{\min}$ are, respectively, *a, b,* and *c*, the three-phase references for each mode is derived as (13) from (12) in SS1

$$\begin{cases} V_a^{p*} = V_{zs1} \\ V_b^{p*} = V_{zs1} \\ V_c^{p*} = V_{zs1} \end{cases} \tag{13a}$$

$$\begin{cases} V_a^{e*} = 2V_{\max} + V_{zs2} \\ V_b^{e*} = 2V_{\mathrm{med}} + V_{zs2} \\ V_c^{e*} = 2V_{\min} + V_{zs2} \end{cases} \tag{13b}$$

where V_{zs1} and V_{zs2} are zero-sequence voltages.

The switching losses can be changed by how to set V_{zs1} and V_{zs2}. In this paper, V_{zs1} in (13) is set such that all references are placed below the carrier wave for the pivoting mode, whereas V_{zs2} is set for the enclosing mode according to the same principle of SVM [16]. This setting leads to six switching instants per $2T_{\mathrm{samp}}$ for one converter, which is identical to that of the conventional SVM.

The modification by (13) is applied only if (9) is satisfied. Therefore, it is implicitly assumed that $2V_{\max} - 2V_{\min}$ is larger than or equal to V_{dc} in the rest of the subsectors.

Subsector 2 or 3 (SS2 or SS3): $\vec{V}_{\mathrm{co1}}$ in Fig. 11 should be used as a pivot vector in SS2 and SS3. This is because only $\vec{V}_{\mathrm{co0}}$, $\vec{V}_{\mathrm{co1}}$, or $\vec{V}_{\mathrm{co2}}$ can be used as a pivot vector, and these subsectors are closer to $\vec{V}_{\mathrm{co1}}$ than $\vec{V}_{\mathrm{co0}}$ or $\vec{V}_{\mathrm{co2}}$. In addition, $\vec{V}_{\mathrm{co3}}, \vec{V}_{\mathrm{co4}}$, and $\vec{V}_{\mathrm{co5}}$ cannot be used as a pivot vector because they cannot be made by a single converter. However, the meanings of $\vec{V}_{\mathrm{co1}}$ and these subsectors need to be discussed further generally. Namely, $\vec{V}_{\mathrm{co1}}$ in Fig. 11 is used to symbolize SOV, and these subsectors are expected to use an SOV as the pivot vector. Therefore, it is checked by (14) whether these subsectors are related or not

$$2V_{\max} - 2V_{\mathrm{med}} \geq 2V_{\mathrm{med}} - 2V_{\min}. \tag{14}$$

In the voltage plane of $2V_{\max}, 2V_{\mathrm{med}}$, and $2V_{\min}$, the application time of SOV is longer than that of SZV when (14) is satisfied. This is because the application time is proportional to the voltage difference, as shown in Fig. 9. As a result, the space vector satisfying (14) is closer to SOV than SZV, and its pivot vector should be an SOV.

The procedure to specify the three-phase references in (8) begins with the modification shown in the following equation:

$$\vec{V}_X^* = \frac{1}{2T_{\mathrm{mod}}} \frac{T_{\mathrm{mod}}}{V_{\mathrm{dc}}} \left\{ \vec{V}_{\mathrm{sov}} \cdot (2V_{\mathrm{max}} + V_{\mathrm{dc}} - V_{\mathrm{dc}} - 2V_{\mathrm{med}}) \right.$$
$$\left. + \vec{V}_{\mathrm{szv}} \cdot (2V_{\mathrm{med}} + 0 - 0 - 2V_{\mathrm{min}}) \right\}. \tag{15}$$

The above equation is numerically the same as (7), but the format is different. This modification is intended to apply an SOV as the pivot vector and leads to (16). From the first and second terms of the right side in (16), it is evident that only SOV is applied for one T_{mod}

$$\vec{V}_X^* = \frac{1}{2T_{\mathrm{mod}}} \frac{T_{\mathrm{mod}}}{V_{\mathrm{dc}}} \left[\vec{V}_{\mathrm{sov}} \cdot V_{\mathrm{dc}} + \vec{V}_{\mathrm{szv}} \cdot 0 \right.$$
$$+ \vec{V}_{\mathrm{sov}} \{ (2V_{\mathrm{max}} - V_{\mathrm{dc}}) - 2V_{\mathrm{med}} \}$$
$$\left. + \vec{V}_{\mathrm{szv}} (2V_{\mathrm{med}} - 2V_{\mathrm{min}}) \right]. \tag{16}$$

The enclosing mode is then implemented according to the third and fourth terms in (16). However, depending on the polarity of the third term, the enclosing vectors can be either the set of $\vec{V}_{\mathrm{co1}}, \vec{V}_{\mathrm{co3}},$ and $\vec{V}_{\mathrm{co4}}$ (SS2) or the set of $\vec{V}_{\mathrm{co1}}, \vec{V}_{\mathrm{co2}},$ and $\vec{V}_{\mathrm{co4}}$ (SS3) in Fig. 11. Initially, if that polarity is positive, the same SOV and SZV are used for the pivoting and enclosing modes, and the subsector is SS2. Otherwise, the application time of SOV has to be negative in the enclosing mode, but the time cannot be negative. Therefore, a different SOV must be used instead such that its application time is positive.

The method to replace SOV can be derived by modifying (16) according to the following principles. First, because the problem is only with SOV, it is desirable to use the same SZV to minimize a change. Second, as shown in Fig. 8, one SOV can be expressed with the subtraction of the other SOV and SZV. Equation (16) is thus modified into (17) without any numerical change

$$\vec{V}_X^* = \frac{1}{2T_{\mathrm{mod}}} \frac{T_{\mathrm{mod}}}{V_{\mathrm{dc}}} \left[\vec{V}_{\mathrm{sov}} \cdot V_{\mathrm{dc}} + \vec{V}_{\mathrm{szv}} \cdot 0 \right.$$
$$+ (\vec{V}_{\mathrm{szv}} - \vec{V}_{\mathrm{sov}}) \cdot \{ 2V_{\mathrm{med}} - (2V_{\mathrm{max}} - V_{\mathrm{dc}}) \}$$
$$\left. + \vec{V}_{\mathrm{szv}} \cdot \{ 2V_{\mathrm{med}} - 2V_{\mathrm{min}} - 2V_{\mathrm{med}} + (2V_{\mathrm{max}} - V_{\mathrm{dc}}) \} \right]. \tag{17}$$

The above equation is again rearranged into the following equation:

$$\vec{V}_X^* = \frac{1}{2T_{\mathrm{mod}}} \frac{T_{\mathrm{mod}}}{V_{\mathrm{dc}}} \left[\vec{V}_{\mathrm{sov}} \cdot V_{\mathrm{dc}} + \vec{V}_{\mathrm{szv}} \cdot 0 \right.$$
$$+ (\vec{V}_{\mathrm{szv}} - \vec{V}_{\mathrm{sov}}) \cdot \{ 2V_{\mathrm{med}} - (2V_{\mathrm{max}} - V_{\mathrm{dc}}) \}$$
$$\left. + \vec{V}_{\mathrm{szv}} \cdot \{ (2V_{\mathrm{max}} - V_{\mathrm{dc}}) - 2V_{\mathrm{min}} \} \right]. \tag{18}$$

Given that SOV and SZV in (18), respectively, correspond to $\vec{V}_{\mathrm{co1}}$ and $\vec{V}_{\mathrm{co2}}$ in Fig. 11, a reference vector to be synthesized by (18) must belong to SS3.

The modifying method for the optimal PWM appears to be different in SS2 and SS3 when considering (16) and (18). However, when the three-phase references compared to the car-

rier wave are considered, the implementations of (16) and (18) are not different at all. For example, if the phases of $V_{\mathrm{max}}, V_{\mathrm{med}},$ and V_{min} are originally *a, b,* and *c*, then the three-phase references for each mode both in SS2 and SS3 are identically derived as (19). As apparently shown in (19), a modification in the pivoting mode is compensated in the enclosing mode

$$\begin{cases} V_a^{p*} = +V_{\mathrm{dc}} \\ V_b^{p*} = 0 \\ V_c^{p*} = 0 \end{cases} \tag{19a}$$

$$\begin{cases} V_a^{e*} = 2V_{\mathrm{max}} - V_{dc} + V_{zs2} \\ V_b^{e*} = 2V_{\mathrm{med}} + V_{zs2} \\ V_c^{e*} = 2V_{\mathrm{min}} + V_{zs2}. \end{cases} \tag{19b}$$

The adjustment of zero-sequence voltage is meaningful only in the enclosing mode because the vector application is fixed in the pivoting mode. In this paper, the zero-sequence voltage for the enclosing mode both in SS2 and SS3, V_{zs2} in (19b), is simply determined such that the largest one of three-phase reference is equal to V_{dc}.

Subsector 4 or 5 (SS4 or SS5): $\vec{V}_{\mathrm{co2}}$ in Fig. 11 should be used as a pivot vector in SS4 and SS5 because it is closest to these subsectors. In fact, $\vec{V}_{\mathrm{co2}}$ in Fig. 11 is used to symbolize SZV, and these subsectors are expected to use an SZV as the pivot vector. In addition, the correspondence to these subsectors is identified by (20), which is the negation of (14)

$$2V_{\mathrm{max}} - 2V_{\mathrm{med}} < 2V_{\mathrm{med}} - 2V_{\mathrm{min}}. \tag{20}$$

A similar modification can be made in (8) to apply an SZV as the pivot vector. As a result, (21) is derived for SS4 and SS5 like (16) for SS2 and SS3

$$\vec{V}_X^* = \frac{1}{2T_{\mathrm{mod}}} \frac{T_{\mathrm{mod}}}{V_{\mathrm{dc}}} \left[\vec{V}_{\mathrm{sov}} \cdot 0 + \vec{V}_{\mathrm{szv}} \cdot V_{\mathrm{dc}} \right.$$
$$+ \vec{V}_{\mathrm{sov}} \cdot (2V_{\mathrm{max}} - 2V_{\mathrm{med}}) + \vec{V}_{\mathrm{szv}}$$
$$\left. \cdot \{ 2V_{\mathrm{med}} - (2V_{\mathrm{min}} + V_{\mathrm{dc}}) \} \right]. \tag{21}$$

As expected from (19), the three-phase references compared to the carrier wave are identically calculated both for SS4 and SS5. Namely, if the phases of $V_{\mathrm{max}}, V_{\mathrm{med}},$ and V_{min} are originally *a, b,* and *c*, then the three-phase references for each mode both in SS4 and SS5 are identically derived as (22)

$$\begin{cases} V_a^{p*} = V_{\mathrm{dc}} \\ V_b^{p*} = V_{\mathrm{dc}} \\ V_c^{p*} = V_{\mathrm{dc}} - V_{\mathrm{dc}} = 0 \end{cases} \tag{22a}$$

$$\begin{cases} V_a^{e*} = 2V_{\mathrm{max}} + V_{zs2} \\ V_b^{e*} = 2V_{\mathrm{med}} + V_{zs2} \\ V_c^{e*} = 2V_{\mathrm{min}} + V_{\mathrm{dc}} + V_{zs2}. \end{cases} \tag{22b}$$

The adjustment of zero-sequence voltage is also meaningful only in the enclosing mode. In this paper, the zero-sequence voltage for the enclosing mode in SS4 and SS5, V_{zs2} in (22-b), is simply determined, such that the largest one of three-phase reference is equal to V_{dc}.
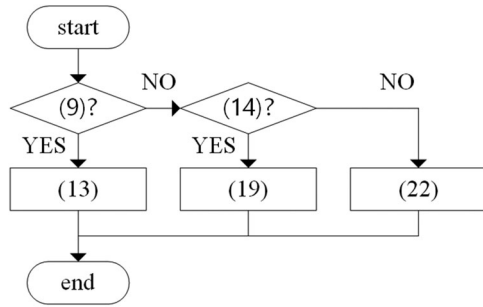
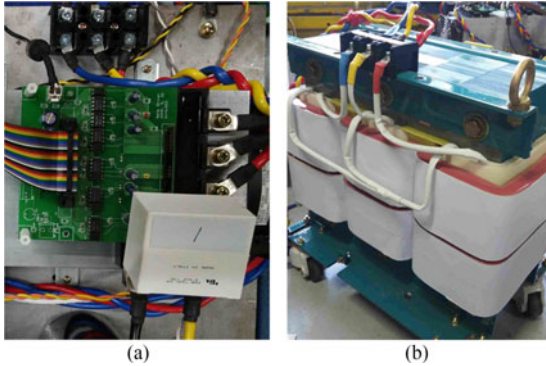Fig. 12. Flowchart to modify voltage references for each converter.

Fig. 13. Experimental setup: (a) converter; and (b) transformer.
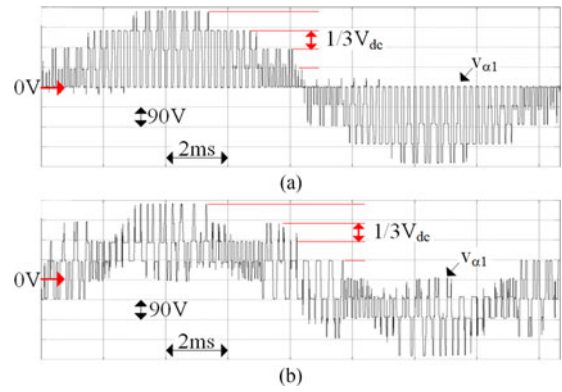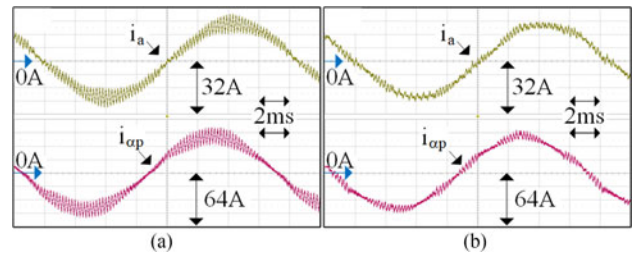

Fig. 14. Voltage waveform of α_1 winding: (a) conventional method; and (b) proposed method.

Fig. 15. Current waveforms: (a) conventional method; and (b) proposed method.

Finally, the proposed method to modify voltage references for CNV_X can be summarized as a flowchart in Fig. 12. Before starting the process of Fig. 12, it is assumed that the phases of $V_{\max}, V_{\mathrm{med}}$, and $V_{\min}$ have already been identified as *a, b,* and *c*, respectively. According to the flowchart in Fig. 12, the three-phase references for each mode are calculated by (13), (19), or (22). The same procedure shown in Fig. 12 is also applied to CNV_Y. Finally, calculated references are then synthesized as explained in Fig. 10 for each converter.

The simple methods to set zero-sequence voltage have been detailed for each case when (13), (19), and (22) are considered. Although it is an important issue how to optimize those methods for harmonic properties and switching losses, it is beyond the scope of this paper. However, it should be noted that the total number of switching instants per $2T_{\mathrm{samp}}$ was virtually six with respect to three-phase references by the aforementioned settings. That is, the effective switching frequency of the proposed method is almost identical to that of the conventional PWM.

IV. EXPERIMENTAL RESULTS

Experiments were planned to examine the effectiveness of the proposed method and executed with two converters, one of which is shown in Fig. 13(a). Those converters were based on the intelligent power module (IPM) including six insulated gate bipolar transistors (IGBTs) for a three-phase converter. The gating signals were made by the control board based on TMS320C28346 and transferred to the inputs of IPMs. For comparison, the conventional and proposed PWM methods were digitally implemented in the control board.

First, the proposed method was tested with a 6-kVA DDSW-based transformer shown in Fig. 13(b), whose primary wye-connected windings were connected to an 110 V-60 Hz grid. Because the system operated to emulate an energy storage system whose battery was fully charged, the dc-link of each converter was set to 260 V. In addition, the switching frequency of both the conventional and proposed methods was set low at 2.5 kHz to emulate a multi mega-watt system.

The employment of voltage levels during PWM needs to be checked because its optimization is crucial in the proposed method. The winding voltages were then captured for each method as shown in Fig. 14, and the notation for voltage and current in experimental results hereafter is following that in Fig. 3. In the comparison between Fig. 14(a) and (b), the employment of voltage levels was definitely changed by the proposed method. However, it is not easy to figure out with Fig. 14 how optimal the proposed method is. This is because the optimization was initially intended for PWM of the combined voltage. In fact, the winding voltages shown in Fig. 14 is not the direct target to be optimized.

The optimization effect can be indirectly confirmed through the current flowing at the primary side because its harmonics are affected by the combined voltage's PWM, as explained in (1) and Fig. 4. The current flowing at the primary side $(i_{\alpha p})$ is shown in Fig. 15, and it is conspicuous how effective the proposed method mitigates ripples at the switching frequency. When the fundamental of $i_{\alpha p}$ was about 43 A, its total harmonic distortion (THD) was decreased from 13.4% to 7.6% by virtue of the proposed method. In addition, it is noticeable in Fig. 15 that current ripples at the secondary side were also quite reduced by the proposed method. When the fundamental of i_a was about 22 A, its THD was decreased from 13.4% to 8.3%. Therefore, it is summarized that the proposed optimization for the primary side has also resulted in an improvement for the secondary side.
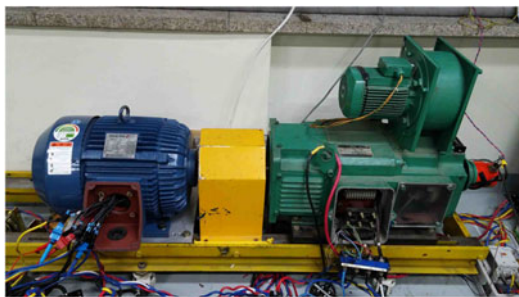
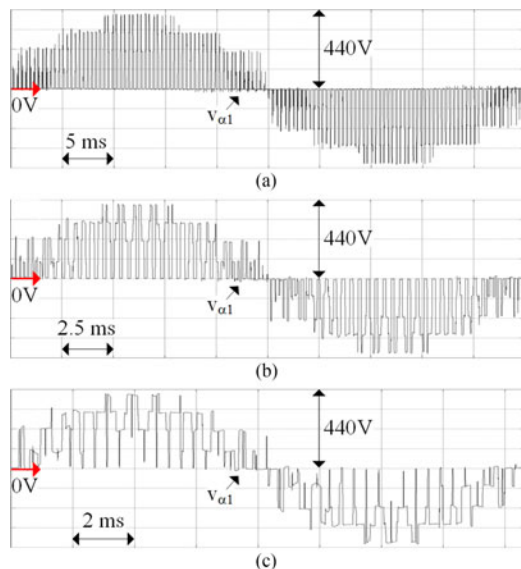Fig. 16.   Setup to test DDSW-based machine: (left) test machine and (right) load machine.

Fig. 17.   Winding voltage by conventional method when MI is (a) 0.33, (b) 0.66, and (c) 0.99.
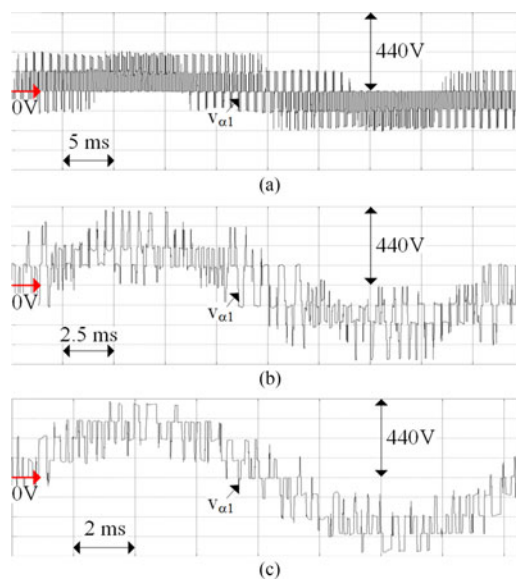

Fig. 18.   Winding voltage by proposed method when MI is (a) 0.33, (b) 0.66, and (c) 0.99.
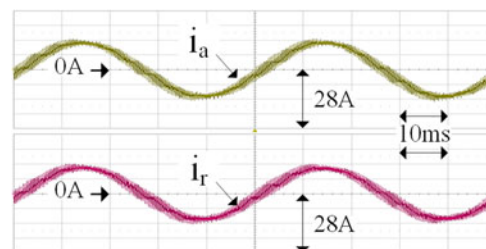

Fig. 19.   Converter currents to induction machine by the conventional method when MI is 0.33.
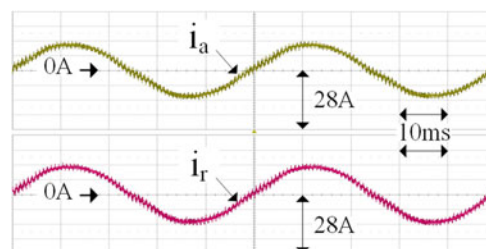

Fig. 20.   Converter currents to induction machine by the proposed method when MI is 0.33.

The effect of the proposed method was also considered when the modulation index (MI) changes, which is defined as the ratio of voltage magnitude to $V_{dc}/\sqrt{3}$ in this paper. The case shown in Figs. 14 and 15 was under MI of 0.67 V/V. Since a wide range of MIs were limited with the transformer experiment, an 11-kW dual-winding induction machine shown in Fig. 16 was used for experiments. This machine was a commercial product for dual voltage operation, either 220 V or 440 V, and the dc-link voltage of each converter was aptly set to 315 V for DDSW operations. In addition, the switching frequency was set at 1.25 kHz to show evident differences in harmonics. In order to change MI, the test machine was driven by V/f control at 20, 40, and 60 Hz under no load. Since back electromotive force was proportional to the operating frequency, the MIs for each case were 0.33, 0.66, and 0.99, respectively.

The improvement of the waveform with the proposed method is remarkable under these MI-varying experiments even with observing the winding voltages, which are indirectly affected by the proposed method. At first, as shown in Fig. 17, the employment of voltage levels was quite consistent in the conventional method except that the relative period of PWM was changed with respect to the fundamental period. However, the employment of voltage levels was conspicuously changed in the proposed method for adapting to the MI-variation, as shown

in Fig. 18. Through this comparison, it can be inferred that the proposed method works better by using the closer voltage-levels to the fundamental voltage. This point would be very helpful in high-power motor drives because it could minimize the problems such as excessive voltage stress on windings, motor leakage currents, electromagnetic interference, etc. [18].

In addition, the proposed PWM method has also resulted in smaller current-ripples for the test machine as expected. This point can be confirmed with Figs. 19 and 20, where the converter currents at the same phase are shown simultaneously. For a precise analysis, the frequency spectrums of the converter currents can be compared as shown in Fig. 21. By virtue of the proposed method, the ripples near 2.5 kHz (double the
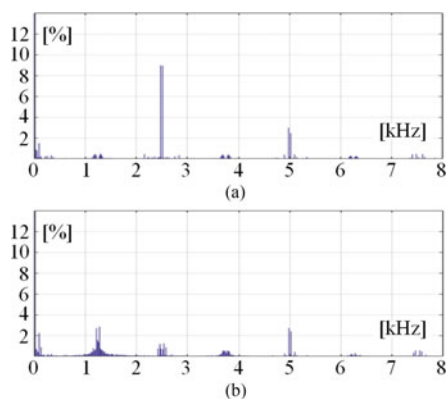
Fig. 21. Frequency spectrum of converter currents when MI is 0.33: (a) conventional method; and (b) proposed method.

switching frequency) was quite reduced even if that near 1.25 kHz (the switching frequency) was little bit increased.

V. Conclusion

In this paper, a novel method to optimize PWM in DDSW-based systems has been proposed. In detail, the aim was to minimize excessive usage of voltage levels during PWM, and the strategy was to divide the roles of each converter to use the nearest space vectors. The implementation scheme of PWM has been derived by using several general concepts and their mathematical equations. In order to discuss the effectiveness of the proposed method, two types of experimental setups have been devised, and the experimental results have been analyzed with voltage and current waveforms. By virtue of the proposed method, it has been shown that voltage and current harmonics of switching frequency could be conspicuously reduced over the entire system. In particular, current harmonics of concern have been diminished by 40% through the proposed optimization. The contents of this paper were previously disclosed in [19] and revised for better understanding.

References

[1] Y. Park, S. Ohn, and S.-K. Sul, "Multi-level operation with two-level converters through a double-delta source connected transformer," *J. Power Electron.*, vol. 14, no. 6, pp. 1093–1099, Nov. 2014.

[2] Y. Park, J.-M. Yoo, and S.-K. Sul, "Current regulation and fault tolerance in double-delta sourced transformer," in *Proc. 2015 IEEE Energy Convers. Congr. Expo.*, Montreal, QC, Canada, 2015, pp. 1541–1548.

[3] Y. Park, J.-M. Yoo, and S.-K. Sul, "Vector control of double-delta sourced winding for a dual-winding induction machine," *IEEE Trans. Ind. Appl.*, vol. 53, no. 1, pp. 171–180, Jan./Feb. 2017.

[4] S. Brisset, D. Vizireanu, and P. Brochet, "Design and optimization of a nine-phase axial-flux PM synchronous generator with concentrated winding for direct-drive wind turbine," *IEEE Trans. Ind. Appl.*, vol. 44, no. 3, pp. 707–715, May/Jun. 2008.

[5] F. B. Grigoletto and H. Pinheiro, "Flexible arrangement of static converters for grid-connected wind energy conversion systems," *IEEE Trans. Ind. Electron.*, vol. 61, no. 9, pp. 4707–4721, Sep. 2014.

[6] E. Cengelci, P. N. Enjeti, and J. W. Gray, "A new modular motor-modular inverter concept for medium-voltage adjustable-speed-drive systems," *IEEE Trans. Ind. Appl.*, vol. 36, no. 3, pp. 786–796, May/Jun. 2000.

[7] S. Schroder *et al.*, "Modular high-power shunt-interleaved drive system: A realization up to 35 MW for oil and gas applications," *IEEE Trans. Ind. Appl.*, vol. 46, no. 2, pp. 821–830, Mar./Apr. 2010.

[8] *IEEE Standard for Interconnecting Distributed Resources With Electric Power Systems*, IEEE Std. 1547, 2003.

[9] J. D. Glover, M. S. Sarma, and T. J. Overbye, "Three-winding transformers," in *Power System Analysis and Design*. Stamford, CT, USA: Cengage Learn., 2012, ch. 3.6, pp. 126–130.

[10] K. Zhou and D. Wang, "Relationship between space-vector modulation and three-phase carrier-based PWM: A comprehensive analysis," *IEEE Trans. Ind. Electron.*, vol. 49, no. 1, pp. 186–196, Feb. 2002.

[11] Y. Park, S.-K. Sul, C.-H. Lim, W.-C. Kim, and S.-H. Lee, "Asymmetric control of DC-link voltages for separate MPPTs in three-level inverters," *IEEE Trans. Power Electron.*, vol. 28, no. 6, pp. 2760–2769, Jun. 2013.

[12] D. Casadei, G. Grandi, A. Lega, and C. Rossi, "Multilevel operation and input power balancing for a dual two-level inverter with insulated DC sources," *IEEE Trans. Ind. Appl.*, vol. 44, no. 6, pp. 1815–1824, Nov./Dec. 2008.

[13] G. Grandi, C. Rossi, D. Ostojic, and D. Casadei, "A new multilevel conversion structure for grid-connected PV applications," *IEEE Trans. Ind. Electron.*, vol. 56, no. 11, pp. 4416–4426, Nov. 2009.

[14] J. Holtz, W. Lotzkat, and A. M. Khambadkone, "On continuous control of PWM inverters in the overmodulation range including the six-step mode," *IEEE Trans. Power Electron.*, vol. 8, no. 4, pp. 546–553, Oct. 1993.

[15] Y. Park, S. K. Sul, and K. N. Hong, "Linear overmodulation strategy for current control in photovoltaic inverter," *IEEE Trans. Ind. Appl.*, vol. 52, no. 1, pp. 322–331, Jan./Feb. 2016.

[16] D.-W. Chung, J.-S. Kim, and S.-K. Sul, "Unified voltage modulation technique for real-time three-phase power conversion," *IEEE Trans. Ind. Appl.*, vol. 34, no. 2, pp. 374–380, Mar./Apr. 1998.

[17] H. W. van der Broeck, H. C. Skudelny, and G. V. Stanke, "Analysis and realization of a pulsewidth modulator based on voltage space vectors," *IEEE Trans. Ind. Appl.*, vol. 24, no. 1, pp. 142–150, Jan./Feb. 1988.

[18] L. Palma and P. Enjeti, "An inverter output filter to mitigate dv/dt effects in PWM drive system," in *Proc. 7th Annu. IEEE Conf. Appl. Power Electron. Conf. Expo.*, 2002, pp. 550–556.

[19] Y. Park and S.-K. Sul, "Pulsewidth modulation strategy in double-delta sourced winding," in *Proc. 2016 IEEE Energy Convers. Congr. Expo.*, Milwaukee, WI, USA, 2016, pp. 1–8.

Yongsoon Park (S'12–M'15) received the B.S., M.S., and Ph.D. degrees in electrical engineering from Seoul National University, Seoul, South Korea, in 2008, 2010, and 2015, respectively.

From 2015 to 2016, he was a Senior Engineer with Samsung Electronics Company, Ltd., Suwon, South Korea. Since 2016, he has been with the Gwangju Institute of Science and Technology, Gwangju, South Korea, where he is currently an Assistant Professor. His research interests include design and control of power conversion circuits for grid connection and motor drives.

Seung-Ki Sul (S'78–M'87–SM'98–F'00) received the B.S., M.S., and Ph.D. degrees in electrical engineering from Seoul National University, Seoul, South Korea, in 1980, 1983, and 1986, respectively.

From 1986 to 1988, he was an Associate Researcher in the Department of Electrical and Computer Engineering, University of Wisconsin–Madison, Madison, WI, USA. From 1988 to 1990, he was a Principal Research Engineer at the LG Industrial Systems Company, Cheongju, South Korea. Since 1991, he has been a Member of Faculty with the School of the Electrical and Computer Engineering, Seoul National University, where he is currently a Professor. He was the author or co-author of more than 150 IEEE journal papers and more than 340 international conference papers in the area of power electronics. He holds 14 U.S. patents, seven Japanese patents, and 11 Korean patents, and has granted 43 Ph.Ds under his supervision. His research interests include power electronic control of electrical machines, electric/hybrid vehicles and ship drives, high-voltage dc transmission based on Modular Multilevel Converter, and power-converter circuits for renewable energy sources.

Prof. Sul was the Program Chair of IEEE Power Electronics Specialist Conference'06 and the General Chair of IEEE Energy Conversion Congress and Exposition-Asia, International Conference on Power Electronics, 2011. In 2015, he was the President of The Korean Institute of Power Electronics. He was the recipient of 2015 IEEE Transaction 1st and 2nd paper awards on Industry Applications, simultaneously. He was also the recipient of the 2016 Outstanding Achievement Award of the IEEE Industry Applications Society and the 2017 Newell award from the IEEE Power Electronics Society.